The role of the recombination centers on the modulated photocurrent: Determination of the gap state parameters of semiconductors

Maura Pomoni, Athina Giannopoulou, P Kounavis

The role of the recombination centers on the modulated photocurrent: Determination of the gap state parameters of semiconductors

Journal:	*Philosophical Magazine & Philosophical Magazine Letters*
Manuscript ID:	TPHM-09-Dec-0503.R1
Journal Selection:	Philosophical Magazine
Date Submitted by the Author:	12-Apr-2010
Complete List of Authors:	Pomoni, Maura; University of Patras, Department of Engineering Sciences Giannopoulou, Athina; University of Patras, Department of Engineering Sciences KOUNAVIS, P; University of Patras
Keywords:	semiconductors, photoelectrical, modelling, numerical simulation, thin films
Keywords (user supplied):	

The role of the recombination centers on the modulated photocurrent: Determination of the gap state parameters of semiconductors

M. Pomoni, A. Giannopoulou, P. Kounavis*

Department of Engineering Sciences, School of Engineering,

University of Patras, 26504 Patra, Greece

Exact expressions of the out of phase modulated photocurrent (MPC), the so-called Y signal, with a clear physical insight for a density of states (DOS) spectroscopy are derived without any approximation. It is found that apart from the capture rate of the majority carriers into the probed gap states, additional mixed contributions **from the recombination processes of the free majority carriers with trapped minority carriers** may be important for the Y signal of lower frequencies. The above additional contributions prevent the extraction of a reliable DOS. They become important as far as the capture coefficient for the majority carriers of the recombination centers where the minority carriers are trapped is comparable or higher than that of the recombination centers were the majority carriers are trapped. In this case, the recombination rate is relatively high and the mixed contributions from the recombination processes can be detectable in the experimental Y signal and may also induce a phase lead. Taking advantage of this behavior **it can be experimentally verified when these recombination processes are negligible in order to safely extract the accurate DOS parameters.**

PACS numbers: 71.25.Mg, 71.55.Jv, 73.50.Gr

*Electronic address: pkounavis@des.upatras.gr

I. INTRODUCTION

The modulated photocurrent (MPC) technique has been applied to determine the density of states (DOS) in the energy gap of various semiconductors including crystalline [1–3], amorphous [4–10], microcrystalline [11], quasicrystalline [12] as well as organic [13, 14] semiconductors. **This technique is very powerful as it can reveal even very low trap densities, as well as the capture coefficients. The experimental setup as is demonstrated in the sketch of Fig.1(a) is simple and requires relatively cheap equipment. In this experiment a semiconductor film with ohmic electrodes in coplanar geometry is illuminated by two light emitted diodes (LED's) of band gap light. The one LED provides a relatively weak sinusoidally modulated light (see Fig.1(b)) of angular modulation frequency ω generating the MPC. The second LED provides a moderate bias light generating a constant photocurrent. The MPC is amplified by a low noise current amplifier close to the sample to minimize stray capacitance. The output from the amplifier is analyzed by a Lock-in amplifier, which provides the amplitude, i_{ac}, of the MPC and the phase shift, ϕ, between the MPC and the modulated light (see Fig.1(b)), which may be a phase lag [1, 5–8] or a small phase lead [15] . The theoretical analysis of the MPC data is based on the multiple trapping model and the derived basic expressions indicate two different regimes:** that at high frequencies (ω) and/or low bias light levels, the so-called high frequency (HF) or emission-limited regime and that at low frequencies and/or high bias light levels, the so-called low frequency (LF) or trapping-limited regime.

Simple theoretical expressions with a physical insight into the MPC data have been originally presented in 1981 by Oheda [1] for the HF regime, which is typically a small portion of the experimental spectra at higher ω. **Based on this analysis Bruggemann et al [6] in 1990 proposed a formula for the determination of the so-called reduced DOS (r-DOS), $(c/\mu)D(E_\omega)$. This formula provides by means of the i_{ac} and ϕ data the r-DOS at the probe energy level E_ω for which the thermal emission rate of the majority carriers equals the modulation frequency ω. Thus by scanning ω [8, 16–18] the DOS at different E_ω levels can be obtained. This method is applicable exclusively for the MPC data in the HF regime. Various attempts have been made to extract information about the DOS and to determine the usually unknown ratio of the capture coefficient to the mobility of the predominated carriers, c/μ, by means of the MPC data of lower ω [9, 19–30].** However, the general

analytical expressions originally derived by Longeaud and Kleider [19] in 1992 and Hattori et al [20] in 1994 are very complicated to extract a simple relation between the MPC of lower ω and the DOS. For this reason an empiric expression was derived by Hattori et al [20] which was applied to determine the DOS parameters of a-Si:H by means of the MPC data obtained upon scanning the bias light level. During this scan the probe energy level (E_ω) was assumed *a-priori* fixed. Subsequently, in 2001 we presented a general theoretical analysis of the MPC [31] where it was shown that the E_ω level can be shifted not only by the modulation frequency, but also by the bias light level. This result invalidates [32] the basic assumption of the method of Hattori et al. In our theoretical analysis [31] a simple approximate expression of the out of phase MPC signal, the so-called Y signal, was extracted. **The Y signal was approximated by** the capture rate of the majority carriers into the probed gap states for any frequency. This is the basis of our DOS spectroscopy, which has the advantage that it can be used to extract the capture coefficients and the density of the probed states by means of the i_{ac} and ϕ data of any ω, including those at lower ω which were not utilized before [32–36]. Later, in 2002 Koropecki et al [37] of INTEC group and in 2004 Guenier et al [38] of LGEP group concentrated their analysis on the LF regime in which the expressions of the MPC take a relatively simpler form. They arrived to similar approximate formulas differing in the proportionality constant for the calculation of the DOS.

The above mentioned methods are based on specific assumptions which result to different simplified approximate expressions relating the MPC data with a specific probed DOS. However, the validity and the limitations of these approximations have been not extensively explored. Moreover, it was not specified when a reliable DOS can be extracted from a given set of MPC data. Recently, different studies have been devoted on the accuracy of the DOS determined from the MPC data by means of model simulations [40–42]. It was deduced that the capture coefficients of the gap states are important for the MPC, without to exactly understand their role [42]. Moreover, an unexplained phase lead has been obtained both experimentally and by simulations [15].

This work concerns a theoretical analysis of the MPC concentrated on the above addressed issues. Specifically, simple exact analytical expressions are derived in Sec.II without any approximation describing all the physical processes contributing to the MPC. It is demonstrated when and how the accurate gap state parameters can be safely extracted from a given set of MPC data. All the theoretical predictions are confirmed by means of model simulations in Sec.III and compared with experimental observations in Sec.IV.

II. THEORETICAL ANALYSIS

A. Basic expressions

The expressions of the free electron and hole modulated densities n_{ac} and p_{ac}, respectively, have been extracted in our first analysis and are given by Eqs.(B3) and (B4) of Ref.[31], respectively. It is proved convenient to express them in the form $n_{ac} = G_{ac}/(X_n + jY_n)$ and $p_{ac} = G_{ac}/(X_p + jY_p)$, where j is the imaginary unit, $Y_{n,p}$ and $X_{n,p}$ are the imaginary and real parts of the denominators of the Eqs.(B3) and (B4) of Ref.[31] and G_{ac} is the modulated light generation rate. The experimental i_{ac}, ϕ data, which are expressed in terms of the real and imaginary parts of n_{ac} and p_{ac} (see Eqs.(24) and (25) of Ref.[31]), can be used to directly calculate the Y signal by means of

$$Y = \mu e G_{ac} \frac{\sin\phi}{\sigma_{ac}}, \tag{1}$$

where μ is the mobility of the predominant carriers and σ_{ac} is the modulated photoconductivity calculated from i_{ac}. The so-calculated Y signal from the experimental data is the essential parameter of the MPC experiment, because it may be directly proportional to the probed DOS ($D(E_\omega)$) for any frequency [31].

Specifically, we have shown that the Y signal may coincide with the imaginary part Y_n (Y_p), when electrons (holes) dominate. **Unlikely, only an approximate expression of the above imaginary part has been obtained in our first analysis [31] relating the Y signal with the probed DOS ($D(E_\omega)$). Here the exact expression of this imaginary part is obtained without any approximation.** For this purpose several species of monovalent gap state $D^i(E)$ distributions are considered with different capture coefficients c_n^i and c_p^i for the electrons and holes, respectively. This is because the energy gap consists of gap states of different origin, whereas the charge state of a given localized state is altered following a carrier capture. The electrons are assumed throughout this analysis as the majority carriers. Hence we concentrate on the exact expression of the Y_n, which is the imaginary part of the denominator of the exact expression of n_{ac} of Eq.(B3) of Ref.[31] derived without any approximation. For this purpose the factor K, which is given by Eq.(A1) in the Appendix and appears in the exact expression of n_{ac}, is replaced by its imaginary K_{im} and real K_{re} parts. The derived Y_n is expressed by three components as

$$Y_n \cong Y_{1n} + Y_{2n} + Y_{3n}, \tag{2}$$

where

$$Y_{1n} = \sum_i \int_{E_V}^{E_C} d_n^i(E) b_{\omega n}^i(E) c_n^i D^i(E) dE, \quad (3)$$

$$Y_{2n} = \sum_i \int_{E_V}^{E_C} d_n^i(E) g^i(E) b_{\omega p}^i(E) c_p^i D^i(E) dE, \quad (4)$$

$$Y_{3n} = \sum_i \int_{E_V}^{E_C} d_n^i(E) q_n^i(E) c_n^i D^i(E) dE. \quad (5)$$

In Eqs.(3)-(5) the following functions appear

$$b_{\omega n}^i(E) = \frac{\omega r_n^i(E)}{\omega^2 + [S^i(E)]^2}, \quad (6)$$

$$b_{\omega p}^i(E) = \frac{\omega r_p^i(E)}{\omega^2 + [S^i(E)]^2}, \quad (7)$$

$$d_n^i(E) = \frac{n c_n^i + r_n^i(E)}{S^i(E)}, \quad (8)$$

$$q_n^i(E) = \frac{\omega c_p^i [n g^i(E) + p]}{\omega^2 + (S^i(E))^2}, \quad (9)$$

$$g^i(E) = K_{im} S^i(E)/\omega - K_{re}. \quad (10)$$

In the above equations we have $S^i(E) = n c_n^i + p c_p^i + r_n^i(E) + r_p^i(E)$, where $r_n^i(E) = c_n^i N_C kT exp[-(E_C - E)/kT]$ and $r_p^i(E) = c_p^i N_V kT exp[-(E - E_V)/kT]$ are the thermal emission rates of the electrons and holes, respectively, from a gap energy level E and kT is the thermal energy. E_V and E_C is the conduction and valence band edge where the effective DOS is N_C and N_V, respectively. **The above exact expressions are appropriate to reveal all the physical processes involved in the Y_n and to clarify when it is possible to extract a reliable DOS, as it is explained below.**

B. The cases where a DOS spectroscopy is possible

In the present analysis it is assumed a mobility lifetime product of electrons much higher than that of the holes $\mu_n \tau_n >> \mu_p \tau_p$ and $n >> p$, such that $n c_n^i >> p c_p^i$. Moreover, it is assumed that $Y \cong Y_n$, which is obtained as far as the mobility capture time product of the majority carriers is much higher than that of minority carriers [42]. This way, our analysis is concentrated on the Y_n. A similar analysis holds for the Y_p as far as holes predominate and $Y \cong Y_p$.

The gap states having the higher relative contribution to the Y_n for any frequency are defined by the products $d_n^i(E) b_{\omega n}^i(E)$, $d_n^i(E) b_{\omega p}^i(E)$ and $\omega/(\omega^2 + [S^i(E)]^2)$ which appear in Y_{1n}, Y_{2n} and Y_{3n} of Eqs.(3)-(5), respectively.

These products are illustrated graphically in Figs.2(a) and 2(b), for various modulation frequencies ω by taking $nc_n^i = 99\ s^{-1}$ and $pc_p^i = 1\ s^{-1}$, which give a characteristic frequency $\omega_t^i = nc_n^i + pc_p^i = 100\ rad/s$.

As it is demonstrated in Fig.2(a) (right axis), the first Y_{1n} component is dominated by the **capture rate,** $c_n^i D^i(E)dE$**, of electrons into** the gap states centered at a frequency dependent energy level above midgap. This is the so-called probe energy level of electrons $E_{\omega n}^i$ defined by the respective maximum of the **sharply peaked** $b_{\omega n}^i(E)$ function of Eq.(6) and is given by

$$E_C - E_{\omega n}^i = kTln\left[\frac{c_n^i N_C kT}{\left(\omega^2 + \{\omega_t^i\}^2\right)^{1/2}}\right]. \tag{11}$$

The $b_{\omega n}^i(E)$ **function effectively selects the gap states around the** $E_{\omega n}^i$ **where the thermal emission rate** $r_n^i(E)$ **equals the modulation frequency** ω**. Thus the** $D^i(E_{\omega n}^i)$ **density gives the largest contribution to the** Y_{1n} **and to the quadrature component of the MPC. As a result a delay of the MPC from the modulated light with a phase lag (see Fig.1(b)) is obtained, due to the trapping and thermal release of the electrons into and from probed states at** $E_{\omega n}^i$**. The gap states shallower and deeper than** $E_{\omega n}^i$ **emit trapped electrons faster and slower, respectively, during the modulation period and do not contribute to the phase lag. In the HF regime, taking place for** $\omega >> \omega_t^i$ **the** $E_{\omega n}^i$ **level according to Eq.(11) shifts by the modulation frequency** ω **to shallower energies from the trap quasi Fermi level of trapped electrons** E_{tn}^i**. In the LF regime, taking place for** $\omega << \omega_t^i$**, Eq.(11) predicts that the** $E_{\omega n}^i$ **level is fixed at the** E_{tn}^i **level, which is defined by** $r_n^i(E_{tn}^i) = \omega_t^i$**. In the HF regime the** Y_{1n} **is the only important component and facilitates a DOS spectroscopy. In the LF regime the other two components** Y_{2n} **and** Y_{3n} **may also become important.**

The gap states having the predominant contribution in the Y_{2n} **for the LF regime are mainly selected by the sharply peaked** $b_{\omega p}^i(E)$ **function. These states are shown in Fig.2(a) (thick lines below midgap) and they are centered at the trap quasi Fermi level of holes** E_{tp}^i**, where** $r_p^i(E_{tp}^i) = \omega_t^i$**. In addition, the** Y_{2n} **from Eq.(4) is proportional to the** $g^i(E)$ **of Eq.(10), which contains the real and the imaginary parts of** K**. By considering that both of these parts according to Eqs.(A3) and (A4) of the Appendix are proportional to the** p/n **ratio and using Eq.(8), the** Y_{2n} **for** $\omega << \omega_t^i$ **is found proportional to the** $c_n^i pc_p^i / S^i(E) D^i(E) dE$ **rate. Since the** $pc_p^i / S^i(E)$ **ratio gives the fraction of the unoccupied states, the above rate indicates that the** Y_{2n} **is proportional to the recombination**

rate of free electrons with the trapped holes in the gap states around the E^i_{tp} level. Similarly, in Eq.(5) by taking into account Eq.(9) and Eqs.(A3) and (A4) of the Appendix, the Y_{3n} for the LF regime is also found proportional to the $c^i_n p c^i_p / S^i(E) D^i(E) dE$ rate. The above rate indicates that the Y_{3n} is proportional to the recombination rate of free electrons with trapped holes in the recombination centers of the $D^i(E)$ distributions between the E^i_{tp} and E^i_{tn}. These centers as is evident from Fig.2(b) (thick lines) are selected by the $\omega/(\omega^2 + [S^i(E)]^2)$ ratio in Eq.(9) and they have the largest contribution to the Y_{3n}. This way, the recombination processes involved in Y_{2n} and Y_{3n} may complicate the extraction of a DOS from the data in the LF regime.

It is obvious that the above difficulty may be overcome and an absolute DOS can be extracted by utilizing all the MPC data, as far as the Y_{1n} component predominates in the Y_n and Y signal not only for the HF regime but also for any ω. This way, the probed $D(E_{\omega n})$ dominating in the Y_{1n} can be extracted directly from the Y signal. It is worthy to mention that this possibility can be tested experimentally, because the Y_{1n} has the well defined frequency dependence of the capture rate $1/\tau_{\omega n}$ of electrons into the probe $E_{\omega n}$ level according to

$$Y \cong Y_{1n} \cong \frac{1}{\tau_{\omega n}} = \frac{\pi}{2} H(\omega, \omega_t) c_n D(E_{\omega n}) kT. \tag{12}$$

This relation is obtained from Eq.(3) by considering that Eq.(8) for all the probe $E_{\omega n}$ levels gives $d^i_n(E) \cong 1$ for $nc^i_n >> pc^i_p$ and that the weighting function $b^i_{\omega n}(E)$ can be replaced by a delta function. Eq.(12) has been already derived in our first analysis [31] for the Y_n using an approximation, as is clarified in Sec.II.D. In Eq.(12) the so-called universal H function is given by $H(\omega, \omega_t) = 1 - (2/\pi) arctan(\omega_t/\omega)$, which presents a step at ω_t. **This step generates ultimately a step in the Y signal with a characteristic decay at low ω which can be used to verify experimentally Eq.(12). This decay is due to the fact that the electrons interacting with the probed states at $E_{\omega n}$, which is practically the E_{tn} level at low ω, have an increasingly higher time with decreasing ω to thermal release to the conduction band during a modulation period. This effect results in a decrease of the Y signal and phase shift. Specifically, if $Y \cong Y_{1n}$, then in the HF regime ($\omega >> \omega_t$) we have $H(\omega, \omega_t) \cong 1$, so that according to Eq.(12) all the experimental Y spectra of different bias light levels should merge in the bias light intensity-independent spectrum of $Y_0 \cong \frac{\pi}{2} c_n D(E_{\omega n}) kT$. The experimental Y signal with decreasing ω should start to drop around ω_t from the values of Y_0 following the characteristic decay of the $1/\tau_{\omega n}$ rate, due to the step of H function [31]. This prediction can be experimentally verified,**

because all the parameters c_n, ω_t and $D(E)$ required to calculate the $1/\tau_{\omega n}$ rate from Eq.(12) can be reconstructed from the experimental Y spectra, without any *a-priori* assumption about the DOS. This is illustrated in Sec.III.D by means of simulation examples.

C. The effect of recombination on the Y signal

In the previous section it was deduced that the contributions from the recombination processes governing the Y_{2n} and Y_{3n} should have a negligible contribution to the Y signal, in order for the condition of Eq.(12) to be valid and to extract the DOS. It is then very important to specify the appropriate DOS parameters of the recombination centers which minimize these recombination processes. The exact role of the recombination centers to the dc photoconductivity and MPC can be better clarified by means of a simple DOS model with one valence band-tail like gap state distribution $D^v(E)$ below E_F and another conduction band-tail like gap state distribution $D^c(E)$ above E_F. It is also considered that E_F lies on the minimum where the $D^v(E)$ and $D^c(E)$ overlap, so that these distributions above and below E_F, respectively, vanish and are neglected. This way, it is possible to distinguish the exact role of the characteristics of each $D^v(E)$ and $D^c(E)$.

The charge neutrality condition states that the density of the trapped electrons above E_F equals the density of the trapped holes below E_F. By neglecting the thermal emission rates it becomes

$$\frac{nc_n^c}{nc_n^c + pc_p^c} N_r^c = \frac{pc_p^v}{nc_n^v + pc_p^v} N_r^v, \tag{13}$$

where $N_r^c = \int_{E_F}^{E_{tn}^c} D^c(E)dE$ and $N_r^v = \int_{E_{tp}^v}^{E_F} D^v(E)dE$. It is obvious that the free carriers densities n, p are adjusted to fulfil the above condition, depending on the density of the recombination centers, as well as their capture coefficients. This is more evident from $n/p = (c_p^v/c_n^v)(N_r^v/N_r^c)$ which results from Eq.(13) for $nc_n^i >> pc_p^i$. An important parameter for the photoelectric properties of a photoconductor is the recombination rate, R, which in steady state equals the dc generation rate, G_{dc}, according to

$$R = G_{dc} = \frac{nc_n^v pc_p^v}{nc_n^v + pc_p^v} N_r^v + \frac{nc_n^c pc_p^c}{nc_n^c + pc_p^c} N_r^c. \tag{14}$$

The first and second terms in the right hand side of the above relation indicate that R can be expressed by the capture rate, n/τ_n^v, of the free electrons into the trapped holes **below** E_F and by the capture rate, p/τ_p^c, of the free holes into the trapped electrons **above** E_F, respectively, as is shown schematically in Fig.3. The first

rate dominates, namely, $n/\tau_n^v >> p/\tau_p^c$, because $nc_n^i >> pc_p^i$. Therefore most of the recombination traffic is taking place through the recombination centers below E_F (down arrows in Fig.3), which is practically governed by the c_n^v for a given DOS. By incorporating Eq.(13) in Eq.(14) the lifetimes of electrons and holes defined by $\tau_n = n/G_{dc}$ and $\tau_p = p/G_{dc}$, respectively, are

$$\tau_n = \frac{1}{C_e c_n^c N_r^c}, \tag{15}$$

$$\tau_p = \frac{1}{c_p^v N_r^v}. \tag{16}$$

Thus for a given DOS the capture coefficient, c_n^v, for electrons of the recombination centers where the minority carriers are trapped determines through the parameter $C_e = c_n^v/c_n^c$ the lifetime of electrons τ_n, the photosensitivity [45] and the recombination rate, which is written as

$$R = C_e n c_n^c N_r^c. \tag{17}$$

Note that although the c_p^v affects the p density, it has no net effect in the R and Y_n, because the changes in the c_p^v are counteracted by the induced changes in p. Eqs.(15) and (16) agree with the respective lifetimes of Simmons and Taylor theory [43], except from the parameter C_e in Eq.(15). This parameter is absent in the respective expression of Simmons and Taylor original theory, because the above authors considered constant capture coefficients ($c_n^v = c_n^c$) so that $C_e = 1$.

The approximate Eqs.(A3) and (A4) of K_{im} and K_{re}, derived in the Appendix for the LF regime, are incorporated in the Eqs.(4) and (5) in order to obtain simplified expressions for the Y_{2n} and Y_{3n}. Indeed, by means of the charge neutrality condition of Eq.(13) it is found that the total contribution of the Y_{2n} and Y_{3n} can be expressed by the first component Y_{1n} as $Y_{2n}+Y_{3n} \cong -(C_e/2)Y_{1n}$. **This relation indicates that the total contribution of the Y_{2n} and Y_{3n} is governed by the C_e. This is reasonable, because the Y_{2n} and Y_{3n} are proportional to the recombination rates of free electrons with trapped holes in recombination centers and these rates according to Eq.(17) are governed by C_e. Moreover, the net total $Y_{2n}+Y_{3n}$ contribution appears negative, which indicates that the recombination processes involved in the Y_{2n} and Y_{3n} are associated to a phase lead.** Therefore in the LF regime the Y_n depends on the ratio of the capture coefficients for the majority carriers $C_e = c_n^v/c_n^c$ according to the simple relation

$$Y \cong Y_n \cong (1 - \frac{C_e}{2})Y_{1n}, \tag{18}$$

which is verified by means of simulations in Sec.III.C for $nc_n^i >> pc_p^i$. Similar arguments can be made for the Y_p, as far as holes are the majority carriers. In this case, the crucial parameter is the $C_h = c_p^c/c_p^v$.

Therefore for $C_e << 2$ the recombination rate is sufficiently low and according to Eq.(18) the recombination processes involved in Y_{2n} and Y_{3n} are practically kept negligible to Y_n for the LF regime as well. This results in the condition of Eq.(12), allowing a DOS spectroscopy. By contrast, for $C_e > 2$ according to Eq.(18) the negative total contribution from the recombination processes involved in the Y_{2n} and Y_{3n} dominates giving rise to a negative sign for the Y_n and Y signal and a phase lead (see Fig.1(b)). A phase lead has been also reported by other authors by means of experimental data [15] and simulations without to clarify the exact underlying mechanism [40].

D. Comparison with previous analysis

The second Y_{2n} and third Y_{3n} components of the imaginary part Y_n of the majority carriers derived in the present analysis are missing from our first theoretical analysis [31]. This is because it was considered that the factor K defined by Eq.(A1) in the Appendix, which is important only for the expressions of the MPC in the LF regime, can be approximated by the ratio of the free carriers dc densities p/n, whereas its imaginary part was neglected. Note that these approximations are supported by Eqs.(A3) and (A4) of the Appendix. By incorporating the above approximations, $K_{re} = p/n$ and $K_{im} = 0$, in the exact Eqs.(4) and (5), the Y_{2n} and Y_{3n} in LF regime become zero. This way, the Y_n is described practically by the Y_{1n} of Eq.(12), which also deduced in our first analysis. **However, K_{re} according to Eq.(A3) may be slightly higher or lower than the p/n ratio for which Eq.(5) gives a finite value for Y_{3n}.** In addition, although the K_{im} in the LF regime is negligible compared to the K_{re}, the contribution of the K_{im} in Eqs.(4) and (5) could be not always negligible. This is due to the fact that the K_{im} appears in the above equations as a product with the ratio $S^i(E)/\omega$. This product, taking into account the expression of K_{im} of Eq.(A4) in the Appendix, may be not negligible. Hence the above approximations adopted in our first analysis may be not sufficient to provide a negligible contribution of $Y_{2n} + Y_{3n}$ to Y_n of low ω.

In fact, as it was deduced above the C_e is the crucial parameter and a $C_e << 2$ is required to minimize the contribution of the recombination processes of Y_{2n} and Y_{3n} to Y_n and Y. This important role of the C_e has been not recognized in our first analysis. For simplicity, the Y signal

was simulated for $C_e = 1$ and as a first approximation it was taken in agreement with the $1/\tau_{\omega n}$ of Eq.(12), which in fact is a better approximation for $C_e < 1$ according to Eq.(18) and our recent simulations [42]. In any case Eq.(12), which is the essential restriction of our DOS spectroscopy, should be verified experimentally, in order to safely extract the accurate DOS by means of the general formula extracted in our previous analysis from Eq.(12) [31]

$$D(E_\omega) \cong \frac{2}{\pi} \frac{(Y/\mu)\sigma_p}{e\omega_t H(\omega, \omega_t) kT}. \tag{19}$$

The absolute capture coefficient for the majority carriers can be calculated from $c = e\omega_t\mu/\sigma_p$ by means of the characteristic frequency ω_t, which is extracted according to the procedure described before [31], and the measured dc photoconductivity σ_p, by considering that $\omega_t \cong nc_n$ ($\omega_t \cong pc_p$) when electrons (holes) dominate. The so-derived c can be incorporated in Eq.(11) to obtain the probed trap depths E_ω

$$E_\omega = kTln\left[\frac{(e\omega_t/\sigma_p)\mu N_0 kT}{\left(\omega^2 + [\omega_t]^2\right)^{1/2}}\right], \tag{20}$$

for any ω, by introducing the value for the μN_0 product, where N stands for N_C or N_V.

The analysis originally proposed by the LGEP group [38] and later adopted by the INTEC group for simplicity is based on the hypothesis that the capture coefficients of the gap states for the electrons and holes in the entire energy gap are the same, corresponding to $C_e = 1$. For $C_e = 1$ Eq.(18) reduces to

$$Y \cong Y_n \cong Y_{1n}/2. \tag{21}$$

In the LF regime after a series expansion of H function to the first order gives $H(\omega, \omega_t^i) \cong \frac{2}{\pi}(\frac{\omega}{\omega_t^i})$. In addition, the phase shift, ϕ, is small so that $tan\phi \cong sin\phi$ and $G_{ac}/G_{dc} \cong \sigma_{ac}/\sigma_{dc}$. By introducing these approximations in our Eq.(19) and using Eqs.(1),(12) and (21) we arrive to the simple approximate formula

$$D(E_t) \cong 2\frac{G_{dc}}{kT}\frac{\tan\phi}{\omega}, \tag{22}$$

which was proposed by LGEP group for a DOS spectroscopy. **This formula using all the phase shift (ϕ) data in the LF regime gives a single density, which is the DOS, $D(E_t)$, at the quasi Fermi level of the trapped majority carriers, E_t. This density differs from that calculated with our Eq.(19) using all the i_{ac} and ϕ data in the LF regime** by the factor of 2, due to the factor of 2 in Eq.(21), which is the essential restriction of this method. However, this restriction (obtained with $C_e = 1$) cannot be tested experimentally and the actual DOS cannot be obtained from Eq.(22) in the cases of $C_e < 1$ and $C_e > 1$.

III. MODEL SIMULATIONS

A. Details of simulations

In this section, model simulations are employed in order to verify the theoretical predictions of the previous sections, rather than to fit particular experimental spectra. Moreover, the MPC data generated by the simulations serve as possible experimental data in which our methods are applied to illustrate when and how safe information about the DOS parameters can be extracted. For this purpose we consider the simple DOS model of Fig.4 with the $D^v(E)$ and $D^c(E)$ distributions. These distributions include exponential valence and conduction band-tails with characteristic energies of $E_{ov} = 55$ and $E_{oc} = 35$ meV, respectively. In addition, the $D^v(E)$ and $D^c(E)$ include gaussian distributions, having a maximum density of $3\times10^{17}\ cm^{-3}eV^{-1}$ at 0.56 eV and $1\times10^{16}\ cm^{-3}eV^{-1}$ at 1.28 eV with half-width at half maxima of 0.15 eV and 0.2, respectively. The energy gap is 1.8 eV and the Fermi level is slightly above midgap at 1.0 eV. In this model, the $D^v(E)$ and $D^c(E)$ rapidly vanish above and below E_F, respectively. This way, it is possible to examine the crucial role of the capture coefficient of the recombination centers below and above E_F to the MPC, predicted in Sec.II.C. The capture coefficients are taken as $c_p^v = 10c_n^v = 1\times10^{-7}cm^3s^{-1}$ and $c_n^c = 10c_p^c = 1\times10^{-7}cm^3s^{-1}$ corresponding to negatively ($D^v(E)$) and positively ($D^c(E)$) charged centers, respectively. This model provides that the electrons are the majority carriers giving $n >> p$ such that $nc_n^i >> pc_p^i$. The effect of the C_e parameter on the Y signal predicted in Sec.II is studied by changing the c_n^v keeping fixed the rest parameters.

The simulations were conducted for the fixed temperature of 300 K. Specifically, for a given free electron density n, the respective density p of free holes is numerically obtained by means of the charge neutrality condition [31, 43, 44]. The exact Y spectrum is calculated from Eq.(1) and Eqs.(24), (25) and (B3) of Ref.[31] by means of a simulation code. The accuracy of the numerical results is confirmed by another independent code developed for this purpose.

B. Eventual contributions from the minority carriers

For the DOS model of Fig.4 the DOS above E_F is much lower than that below E_F such that $\tau_{\omega n} >> \tau_{\omega p}$. In our simulations it is considered $\mu_n = 10\mu_p$ so that the mobility capture time product of electrons dominates, namely $\mu_n\tau_{\omega n} >> \mu_p\tau_{\omega p}$. This ensures that $Y \cong Y_n$, as is evident in Fig.5(a). It can be experimentally

confirmed from the fact that the Y signal at higher ω is independent of the bias light level, because H function is unity. By contrast, the experimental Y signal at higher ω is expected to depend on the bias light level in the cases where the Y signal differs from the imaginary part for the majority carriers Y_n for $\mu_n\tau_{\omega n} \leq \mu_p\tau_{\omega p}$, as a result of mixed contributions from the electrons and holes. These are shown in the example of Fig.5(b) obtained upon increasing the mobility of holes at $\mu_p = 10^2\mu_n$ and that of Fig.5(c) obtained upon decreasing both capture coefficients c_p^v and c_n^v of the $D^v(E)$ by a factor of 10^3 lower than the above introduced values so that $\tau_{\omega n} \approx \tau_{\omega p}$. Therefore the behavior of the experimental Y spectra at higher ω can be used to conclude whether these spectra are dominated or not by the imaginary part of the majority carriers (Y_n).

C. Contributions from the probed and recombination states

The behavior of Y signal according to Eq.(18) may depend on the parameter C_e when electrons dominate. This is confirmed in the examples of Fig.6(a) calculated for a fixed $n = 1 \times 10^{10}\ cm^{-3}$ and different C_e obtained upon introducing different values for c_n^v. Specifically, for $C_e < 0.5$ the Y signal has a negligible dependence on the C_e in agreement with Eq.(18) and Y practically agrees with the $1/\tau_{\omega n}$ rate calculated from Eq.(12). This is illustrated in Fig.7(a), which presents Y spectra (solid lines) calculated for $C_e = 0.1$ and generation rates G_{dc} ranging from 2.2×10^{13} to $2.2 \times 10^{18}\ cm^{-3}s^{-1}$. It can be seen the characteristic light intensity-dependent decay of the Y spectra at low ω. This behavior is also usually observed experimentally (see Fig.10(a)) and it can be an indication that the trap-limited conduction mechanism predominates over the alternative hopping transport [46]. Each characteristic decay of Y signal in Fig.7(a) (solid lines) is in excellent agreement with that of $1/\tau_{\omega n}$ rate (triangles) calculated from Eq.(12). As is shown in the example of Fig.7(a) with $n = 10^{10}cm^{-3}$, the Y_{2n} is negative. At low ω the Y_{3n} is positive and counteracts a significant part of the Y_{2n}, so that the $Y_{2n} + Y_{3n}$ is suppressed at very low negative values (see Fig.6(b)). This provides that the Y_{1n} dominates in Y_n, in very good agreement with the prediction of Eq.(18).

Upon increasing C_e, the majority carriers lifetime decreases with only a minor change in the minority carriers lifetime, in very good agreement with the predictions of Eqs.(15) and (16), respectively, as is confirmed in Fig.8(a). This way, as is shown in Fig.8(b), the relative density of

free holes increases compared to that of free electrons, which is kept fixed. In addition, the exact K_{re} agrees with the approximate K_{re} and their small difference from the the p/n ratio, which is not detectable in the graphs of Fig.8(b), is in good agreement with Eq.(A3). In this figure the recombination rate, R, increases with C_e, according to the prediction of Eq.(17). This way, the contributions from the Y_{2n} and Y_{3n} components, which are proportional to recombination rates of free electrons with trapped holes, become both negative for $C_e \geq 0.5$ and increase upon increasing C_e. This is confirmed in Fig.6(b) where for $C_e \geq 0.5$ the maximum of the $-(Y_{2n} + Y_{3n})$ around $\omega_t^c = 10^3\ rad/s$ becomes comparable to the Y_{1n}. Thus the Y signal in Fig.6(a) starts to decay from gradually higher frequencies upon increasing C_e and becomes lower than Y_{1n} according to Eq.(18). This is quantitatively confirmed in Fig.8(c) where the exact Y signal (solid circles) in the LF regime calculated for $\omega = 98\ rad/s$ and various C_e is in excellent agreement with the prediction of Eq.(18) (solid line). It is worthy to mention that as C_e increases, the restriction $nc_n^i >> pc_p^i$ used to derive Eq.(18) may be not valid, particularly at higher C_e. In this case, it was found that only the trend of Y_n is qualitatively described by Eq.(18).

Around $C_e = 2$ a characteristic change in the sign of the Y signal of the LF regime is predicted from Eq.(18) so that for $C_e > 2$ it becomes negative. A remarkable very similar behavior is also confirmed in the examples of the exact Y signal for $C_e > 2$ of Fig.8(c). In this case, the total negative contribution from the $Y_{2n} + Y_{3n}$ exceeds that of the Y_{1n} around $\omega_t^c = 10^3\ rad/s$ and lower ω (see Fig.6(b)). Thus the phase lead from the Y_{2n} and Y_{3n} components dominates over the phase lag from the Y_{1n} at low ω, as is shown in the phase shift spectra of Fig.6(c) with $C_e = 3$ and 6. In this case, the i_{ac} is ahead the modulated light (see Fig.1(b)). This does not mean that the MPC in the output anticipates the modulated light in the input. In fact, as far as the periodic oscillations of the illumination continue unchanged, the MPC is influenced at some finite time in the past by the recombination processes involved in the Y_{2n} and Y_{3n} inducing the phase lead.

D. Determination of the relative contributions to the Y signal and of the DOS parameters

The above analysis showed that only for $C_e < 0.5$ the contributions to the Y signal from the recombination are practically negligible so that reliable DOS parameters can be extracted. This

possibility, as predicted above, can be experimentally verified by comparing the decay of the experimental Y signal around ω_t with that of the $1/\tau_{\omega n}$ rate. Therefore the determination of this rate is crucial. It can be calculated from Eq.(12) by means of the ω_t and $D(E)$, which can be reconstructed from the experimental Y spectra, as is illustrated below with the aid of simulations. The so-calculated rate we call $1/\tau_\omega$ rate, as it is a reconstruction of the actual $1/\tau_{\omega n}$.

The ω_t required for the calculation of the $1/\tau_\omega$ from Eq.(12) can be determined according to the procedure earlier presented [31, 33, 35] which is illustrated with the aid of the simulated example of Fig.7(b). This procedure takes advantage of the fact that for $\omega = \omega_t$ the H function becomes 1/2. This is experimentally evident as a decay in the Y signal by the factor of 2 (vertical arrow) in respect to the value of the Y_0 spectrum with the same trap depth, which corresponds to a frequency higher than ω_t by the factor of $\sqrt{2} = 1.41$ (horizontal arrow). This is because the trap depth of Y, obtained from Eq.(20) for $\omega = \omega_t$, is obtained in the Y_0 spectrum by using $\omega = \sqrt{2}\omega_t$ in Eq.(20), as the characteristic frequency of Y_0 appearing in the denominator of the above equation is practically zero. The so-determined ω_t in the example of Fig.7(b), obtained with $C_e = 0.1$, is in excellent agreement with the actual characteristic frequency ω_t^c (dotted line). From the so-derived ω_t the capture coefficient c_n and the $H(\omega, \omega_t)$ are obtained which are introduced in Eq.(12) to calculate the $1/\tau_\omega$ rate. It is worth mentioning that for the accurate determination of ω_t it is essential to obtain the Y_0 spectrum. The Y_0 in the examples of Figs.7(a) and 7(b) is obtained with an electron density n_0 near dark equilibrium ($n_0 = 2.9 \times 10^6$ cm^{-3}). Unlikely, under this condition the Y_0 spectrum experimentally cannot be obtained at sufficiently high frequencies. As it can be seen from Fig.7(a), the Y_0 spectrum coincides with the upper envelope in which the Y spectra of different bias light levels merge, because in this envelope $H(\omega, \omega_t) \cong 1$. So this envelope can be safely used to experimentally determine the Y_0.

Finally, the $D(E)$ parameter required in Eq.(12) can be obtained from the best fit to the bias light-independent Y_0 spectrum (upper envelope of the Y spectra) using $Y_0 \cong \frac{\pi}{2} c_n D(E_{\omega n}) kT$. This requires to convert the probe trap depths ($E_{\omega n}$) of the $D(E)$ into the respective frequencies by means of Eq.(20) as follows. In the denominator of this equation the respective ω_t for the Y_0 is negligible. In the numerator the μN_0 product can be assumed if it is unknown. For the parameters ω_t and σ_p appearing also in the numerator, the respective values of a moderate bias light level can be used. These values are those from which c_n is calculated. As $D(E)$ is determined, it can be introduced in Eq.(12) to calculate the $1/\tau_\omega$ rate by means of ω_t. Specifically, the extracted ω_t of a given bias

light level is used to determine for any ω the respective probe trap depth $E_{\omega n}$ from Eq.(20) and to specify the respective $D(E_{\omega n})$, which is introduced in Eq.(12).

Upon applying the above described procedure it is reconstructed the $1/\tau_\omega$ rates for all the examples of Y spectra of different C_e, which can be possibly observed experimentally. These rates are plotted in Fig.6(a) (solid lines). In this figure it can be seen that the respective Y signal of Fig.6(a), obtained for $C_e < 0.5$ (open circles and dotted lines) where the total contribution from the Y_{2n} and Y_{3n} is practically negligible (see Fig.6(b)), agrees with the respective reconstructed $1/\tau_\omega$ rate. If such a behavior is experimentally observed, it can be safely concluded that the C_e is relatively low, which provides a low recombination rate, such that $1/\tau_\omega \cong 1/\tau_{\omega n}$. In this case, by applying our methods the actual characteristic frequency and the actual DOS from Eq.(19) are successfully reconstructed. This is confirmed in the examples of Fig.9(a) and Fig.9(b) with $C_e < 0.5$ where it is found that $\omega_t/\omega_t^c \cong 1$ and $D(E) \cong D^c(E)$, respectively. By contrast, the Y signal in the examples of Figs.6(a), obtained for $C_e \geq 0.5$ (solid circles and dotted lines), systematically differs from the respective reconstructed $1/\tau_\omega$ rate. Such an experimental behavior can be used to safely conclude that the $1/\tau_\omega$ differs from the actual $1/\tau_{\omega n}$ and our methods cannot provide the actual DOS parameters. This is due to a relatively high C_e and recombination rate so that the $Y_{2n} + Y_{3n}$ is not negligible (see Fig.6(b)). Indeed, in the examples with $C_e \geq 0.5$, the ω_t in Fig.9(a) significantly overestimates ω_t^c ($\omega_t/\omega_t^c > 1$), whereas in Fig.9(b) the $D(E)$ calculated from Eq.(19) significantly underestimates $D^c(E)$ and does not overlap for different bias light intensities.

We have also applied the methods of the LGEP and INTEC groups to the respective MPC data of the LF regime obtained with the DOS model of Fig.4. The characteristic frequency ω_t, **according to the method proposed by the authors of the above groups [41], is obtained from the frequency where the DOS calculated from Eq.(22) deviates 10% from the respective constant value of the LF regime. This requires to obtain a single DOS value from Eq.(22) by means of all the phase shift data in the LF regime. However, such a single DOS value for every energy is only achieved for $C_e < 2$, as is evident from Fig.9(d). For $C_e \geq 2$ the Y signal presents a steeper decay than the linear decay (see Fig.6(a)). Thus at every energy Eq.(22) gives different values for the DOS by means of the phase shift values of low ω, as in the example of Fig.9(d) for $C_e = 2$. The so-derived DOS parameters**

in Figs.9(c) and 9(d) are close to the actual ones, exclusively for the MPC data of the case of $C_e = 1$, which cannot be experimentally verified. For $C_e < 1$ or $C_e > 1$ the methods of LGEP and INTEC groups cannot provide the actual DOS parameters, as predicted in Sec.II.

IV. COMPARISON WITH EXPERIMENTAL RESULTS

A typical experimental example of Y spectra, which are obtained from the analysis of our MPC data of a-As_2Se_3 sputtered films taken from Fig.1 of Ref.[35], is presented in Fig.10(a). The two Y signals of weak bias illumination levels (open symbols) and the Y signal at higher ω of the moderate bias light level (solid symbols) merge into a single line, defining the bias light intensity-independent Y_0 spectrum. The decay at lower ω of the experimental Y spectrum of the moderate bias light level agrees with the characteristic decay of the $1/\tau_\omega$ rate, reconstructed by means of the Y spectra and Eq.(12) following the procedure described in SecII.D. This agreement is an experimental verification of Eq.(12) predicted for a low $C_{h,e}$ when a unipolar conduction by the majority carriers dominates. A unipolar conduction is indeed taking place by holes [47] in a-As_2Se_3. Moreover, the above films are characterized by a high photosensitivity with a high photo to dark current ratio of the order of 10^3, which is compatible with a low C_h. Therefore the interaction of holes with the probed states dominates in the Y signal of a-As_2Se_3 and the previously extracted [35] DOS parameters from this signal by applying our methods are reliable.

Another characteristic example of experimental Y signal is presented in Fig.10(b). This is obtained from the DOS reported by Kleider et al [24], as calculated from the MPC data of a lightly p-type doped a-Si:H sample. Specifically, the Y spectrum is extracted from the DOS presented in Fig.24(a) of Ref.[24] which was calculated by means of the formula of Bruggenann et al [6]. This formula is equivalent to our Eq.(19) with $H(\omega, \omega_t) = 1$ from which it is evident that the calculated DOS is proportional to Y. Hence this DOS reflects also the Y signal in the energy domain E_ω. By adopting the relation $E_\omega = kTln(\nu_0/\omega)$ with $\nu_0 = 10^{12}s^{-1}$, used by Kleider et al to define the energy scale, the Y signal extracted from the DOS data is converted into the frequency domain ω. The result is presented in Fig.10(b) along with the Y_0 spectrum, which is extracted from the upper envelope of the DOS's of different temperatures. It can be seen that the

Y signal clearly departs from the $1/\tau_\omega$ rate, reconstructed according to the procedure described in SecII.D. This is the predicted behavior for the case where the Y signal is not dominated by the interaction of the majority carriers with the probed states. This conclusion is reasonable for this lightly doped material in which mixed contributions from both carriers are expected, making impossible the extraction of a DOS.

V. CONCLUSIONS

We have obtained general exact expressions for the Y signal without any approximation **which clarify all the physical processes involved in the Y signal. It was illustrated how the predominant of these physical processes can be experimentally detected, by means of examples of simulations and experimental data. Specifically, it was found that mixed contributions from the recombination of free majority carriers with trapped minority carriers may dominate in the Y signal of lower ω and may induce a phase lead complicating the extraction of a DOS.** This is obtained as far as the capture coefficient for the majority carriers of the recombination centers where the minority carriers are trapped is comparable or higher than that of the recombination centers where the majority carriers are trapped, that is for $C_{e,h} \geq 0.5$. This condition for a given DOS favors a relatively lower lifetime for the majority carriers and higher recombination rate. **By contrast, for $C_{e,h} < 0.5$ the mixed contributions from the recombination are negligible, so that the contribution from the capture rate of the majority carriers into the probed states dominates in the Y signal. This can be verified experimentally, because the above capture rate can be reconstructed from the experimental Y spectra. If the reconstructed $1/\tau_\omega$ rate agrees with the Y signal, then this rate dominates in the Y signal and the accurate DOS parameters can be obtained with confidence by our DOS spectroscopy.** It was shown that the methods reported by LGEP and INTEC groups are reliable exclusively for $C_{e,h} = 1$, which unlikely cannot be verified experimentally.

APPENDIX: APPROXIMATE EXPRESSION OF K

The general expression of K appearing in the exact expression of n_{ac} derived in our first analysis [31] (see Eq.(B3)) is given by

$$K = \frac{1 + \sum_i \int_{E_V}^{E_C} \frac{1}{j\omega + S^i(E)} \frac{pc_p^i + r_n^i(E)}{S^i(E)} c_n^i D^i(E) dE}{1 + \sum_i \int_{E_V}^{E_C} \frac{1}{j\omega + S^i(E)} \frac{nc_n^i + r_p^i(E)}{S^i(E)} c_p^i D^i(E) dE}. \tag{A1}$$

This expression is simplified in the LF regime ($\omega << \omega_t^i$) for the case where the gap state distribution $D^c(E)$ dominates above E_F and another gap state distribution $D^v(E)$ dominates below E_F. In the imaginary parts and the real parts of the numerator and denominator of Eq.(A1) some integrals are obtained which are reduced as follows. Specifically, the obtained integrals $\int_{E_V}^{E_C} b_{\omega n,p}^{v,c}(E) c_{n,p}^{v,c} D^{v,c}(E) dE$ to a good approximation can be replaced by $\frac{\pi}{2} H(\omega, \omega_t^{v,c}) c_n^{v,c} D(E_{\omega n,p}) kT$. In the LF regime the probe energy levels $E_{\omega n,p}^{v,c}$ are practically fixed at the respective trap quasi Fermi levels $E_{\omega n,p}^{v,c} \cong E_{tn,p}^{v,c}$ and the H function is approximated as $H(\omega, \omega_t^{v,c}) \cong \frac{2}{\pi} \frac{\omega}{\omega_t^{v,c}}$, so that the above integrals become $\frac{\omega}{\omega_t^{v,c}} c_{n,p}^{v,c} N_{tn,p}^{v,c}$, where $N_{tn,p}^{v,c} = D(E_{tn,p}^{v,c}) kT$. Finally, the obtained integrals $\int_{E_V}^{E_C} \frac{b_{\omega n,p}^{v,c}(E)}{S^{v,c}(E)} c_{n,p}^{v,c} D^{v,c}(E) dE$ can be approximated by $\frac{\omega}{2(\omega_t^{v,c})^2} c_{n,p}^{v,c} N_{tn,p}^{v,c}$.

Upon incorporating the charge neutrality condition (Eq.(13)) presented in Sec.II and defining $g_n = \frac{N_{tn}^c}{N_r^c}$ and $g_p = \frac{N_{tp}^v}{N_r^v}$, the expression of K becomes

$$K \cong \frac{-j\omega(\frac{1}{\omega_t^v} + \frac{1}{2\omega_t^c} g_n) + (1 + g_n)}{-j\omega(\frac{1}{\omega_t^v} + \frac{1}{2\omega_t^v} g_p) + (1 + g_p)} (\frac{p}{n}). \tag{A2}$$

From the above relation the real and imaginary parts of K are obtained for the LF regime in the simple forms

$$K_{re} \cong \alpha_{re} \frac{p}{n}, \tag{A3}$$

$$K_{im} \cong \frac{\omega}{\omega_t^v} \alpha_{im} \frac{p}{n}, \tag{A4}$$

where

$$\alpha_{re} = \frac{1 + g_n}{1 + g_p}, \tag{A5}$$

$$\alpha_{im} = \frac{(1 + g_n)(1 + \frac{g_p}{2}) - (1 + \frac{g_n}{2} \frac{c_n^v}{c_n^c})(1 + g_p)}{(1 + g_p)^2}. \tag{A6}$$

The parameter α_{re} given by Eq.(A5) is usually close to unity for smooth gap state distributions above and below E_F, providing that the quasi Fermi levels are separated by more than a few kT.

REFERENCES

[1] H. Oheda, *J. Appl. Phys.*, **52**, 6693 (1981).

[2] H. Oheda, H. Okushi, H. Tokumaru, and K. Tanaka, *Jap. J. Appl. Phys.*, **20**, L689 (1981).

[3] C. Longeaud, J.,P. Kleider, and M. Cuniot, *Opt. Mater.*, A **294-296**, 519, (2000).

[4] H. Oheda, S. Yamasaki, T. Yoshida, A. Matsuda, H. Okushi, and K. Tanaka, *Jap. J. Appl. Phys.*, **21**, L440 (1982).

[5] G. Schumm and G. Bauer, *Philos. Mag.*, B **58**, 411 (1988).

[6] R. Bruggemann, C. Main, J. Berkin, and S. Reynolds, *Philos. Mag. B*, **62**, 29 (1990).

[7] P. Kounavis and E. Mytilineou, *J. Non-Cryst. Solids*, **137&138**, 955 (1991).

[8] J. P. Kleider, C. Longeaud, and O. Glodt, *J. Non-Cryst. Solids*, **137&138**, 447, (1991).

[9] C. Main, D. P. Webb, R. Bruggemann, and S. Reynolds, *J. Non-Cryst. Solids*, **137&137**, 951 (1991).

[10] P. Kounavis, *J. Non-Cryst. Solids*, **352**, 1068 (2006).

[11] R. Bruggemann, *J. Mater. Science-Materials in Electronics*, **14**, 629 (2003).

[12] M. Takeda, R. Tamura, Y. Sakairi, K. Kimura, *J. Sol. State Chem.,* **133***, 224 (1997)*,

[13] T. Tanaka, M. Mazu, R. Hiroasi, *Thin Sol. Films*, **322**, 290 (1998).

[14] M. Breban, P. B. Romero, S. Mezhenny, V.W. Bollarotto, E. D. Williams, *Appl. Phys. Lett.*, **87**, 203503 (2005).

[15] S. Reynolds, Z. Aneva, Z. Levi, D. Nesheva, C. Main, and V. Smirnov, *J. Non-Cryst. Solids*, **354**, 2744 (2008).

[16] G. Schumm and G. Bauer, *Phys. Rev.*, B **39**, 5311 (1989).

[17] P. Kounavis and E. Mytilineou, *J. Non-Cryst. Solids*, **201**, 119 (1996).

[18] P. Grygiel and W. Tomaszewicz, *J. Phys.: Condens. Matt.*, **12**, 5209 (2000).

[19] J.P. Kleider and C. Longeaud, *Phys. Rev.* B **45**, 11672, (1992).

[20] K. Hattori, Y. Adachi, M. Anzai, H. Okamoto, and Y. Hamakawa, *J. Appl. Phys.*, **76**, 2841 (1994).

[21] P. Kounavis and E. Mytilineou, *J. Non-Cryst. Solids*, **164&166**, 623 (1993).

[22] P. Kounavis, *J. Appl. Phys.*, **77**, 3872 (1995).

[23] P. Kounavis and E. Mytilineou, *Solid State Phenomena*, **44&46**, 715 (1995).

[24] J. P. Kleider and C. Longeaud, *Solid State Phenomena*, **44&46**, 596 (1995).

[25] P. Kounavis, D. Mataras, and D. Rapakoulias, *J. Appl. Phys.*, **80**, 2305 (1996).

[26] P. Kounavis and E. Mytilineou, *Philos. Mag. Lett.*, **72**, 117, (1996).

[27] W. Lauwerence, PhD thesis, Leuven, (1997).

[28] S. Reynolds, C. Main, D. P. Webb, and M. J. Rose, *Philos. Mag.*, B **80**, 547 (2000).

[29] R. Bruggemann and J. P. Kleider. *Thin Solid Films*, **403-404**, 30 (2002).

[30] J. P. Kleider, C. Longeaud, and M. E.Guenier, *Phys. Status Solidi (c)*, **1**, 1208 (2004).

[31] P. Kounavis, *Phys. Rev.*, B **64**, 45204 (2001).

[32] P. Kounavis, *Phys. Rev.*, B **65**, 155207 (2002).

[33] P. Kounavis, *J. Non-Cryst. Solids*, **326-327**, 98 (2003).

[34] P. Kounavis, *Rec. Devel. Physics (Tansworld Research Network)*, **4**, 773 (2003).

[35] P. Kounavis, *Sol. State Comun.*, **131**, 47 (2004).

[36] P. Kounavis, *J. Appl. Phys.*, **97**, 23707 (2005).

[37] R. R. Koropecki, J. A. Schmidt, and R. Arce, *J. Appl. Phys.*, **91**, 8965 (2002).

[38] M. E.Guenier, C. Longeaud, and J. P. Kleider, *Eur. Phys. J. Appl. Phys.*, **26**, 75 (2004).

[39] C. Longeaud, J. A. Schmidt, and J. P. Kleider, *Phys. Rev.*, B **73**, 235316 (2006).

[40] J. A. Schmidt, C. Longeaud, R. R. Koropecki, and R. Arce, *J. Appl. Phys.*, **101**, 103705 (2007).

[41] J. A. Schmidt, C. Longeaud, R. R. Koropecki, and R. Arce, *J. Non-Cryst. Solids*, **354**, 2914 (2008).

[42] M. Pomoni, A. Giannopoulou and P. Kounavis, *J. Non-Cryst. Solids*, **354**, 2238 (2008).

[43] G.W. Taylor and J.G. Simmons, *J. Non-Cryst. Solids*, **8-10**, 940 (1972).

[44] J. Bullot, P. Cordier, M. Gauthier, G. Mawawa, *Philos. Mag.*, **55**, 599 (1987).

[45] R. H. Bube, Photoconductivity of Solids, John Willey & Sons, 1960

[46] C. Longeaud, S. Tobbeche *J. Phys.: Condens. Matter*, **21**, 045508 (2009)

[47] R.A. Street, *Philos. Mag.*, B **38**, 191 (1978).

[48] J. P. Kleider, C. Longeaud, and M. E.Guenier, *J. Non-Cryst. Solids*, **338-340**, 390 (2004).

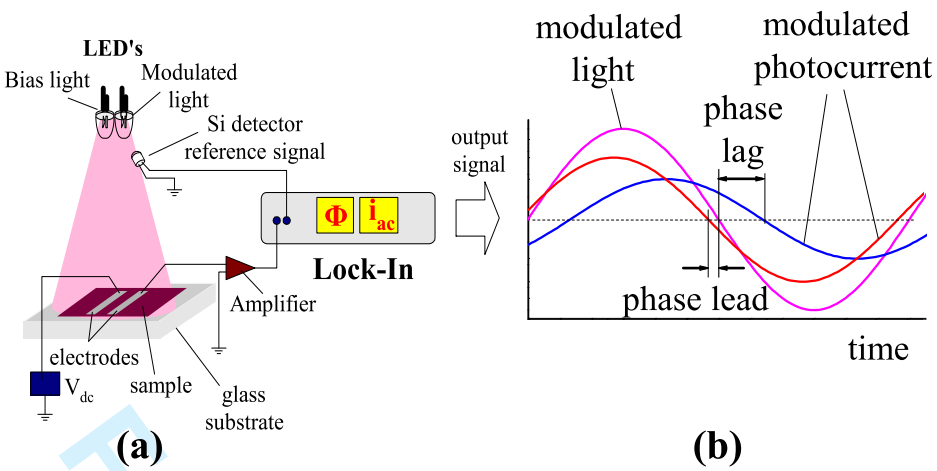

FIG. 1: Sketch showing the experimental setup of the MPC experiment in (a) and evolutions with time of the modulated light and the amplitude of the MPC i_{ac} in (b), where it is illustrated the phase shift, which may be a phase lag or a phase lead.

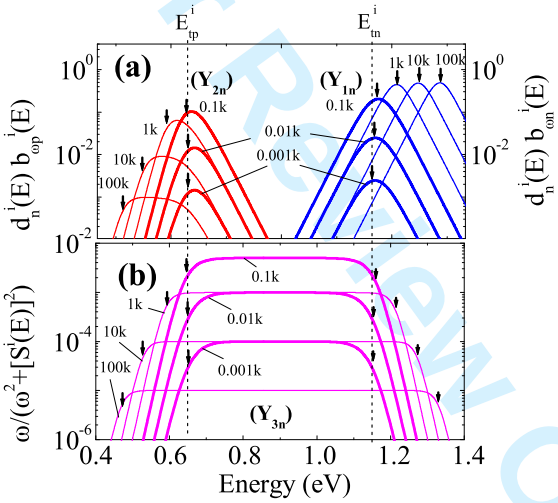

FIG. 2: Energy dependence of the $d_n^i(E)b_{\omega n}^i(E)$ (right axis) and $d_n^i(E)b_{\omega p}^i(E)$ (left axis) products above and below midgap, respectively, in (a) and of the $\omega/(\omega^2 + [S^i(E)]^2)$ ratio in (b) for various ω indicated by the numbers in units of $k = 1000\ rad/s$. These products define the gap states with the higher relative contribution to each component of the Y_n indicated in the parenthesis. The characteristic frequency is at $\omega_t^i = 100 rad/s$ and $c_n^i = c_p^i = 1 \times 10^{-8} cm^3 s^{-1}$. Arrows above and below midgap indicate the $E_{\omega n}^i$ and $E_{\omega p}^i$ levels, respectively. Thinner and thicker lines correspond to $\omega > \omega_t^i$ and $\omega \leq \omega_t^i$, respectively.

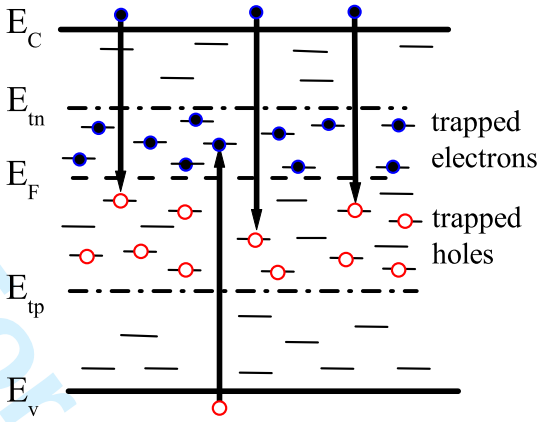

FIG. 3: Recombination processes involving capture of free electrons by trapped holes (down arrows) and capture of free holes by trapped electrons (up arrows). The first process dominates recombination, as the density of trapped electrons and holes are equal and $n >> p$.

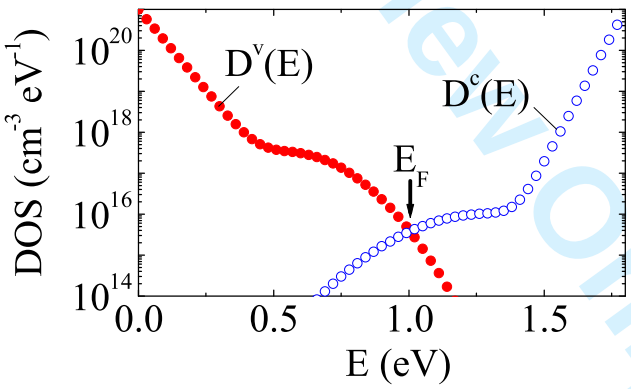

FIG. 4: Gap state distributions $D^v(E)$ (solid circles) and $D^c(E)$ (open circles) of the DOS model introduced in the simulations.

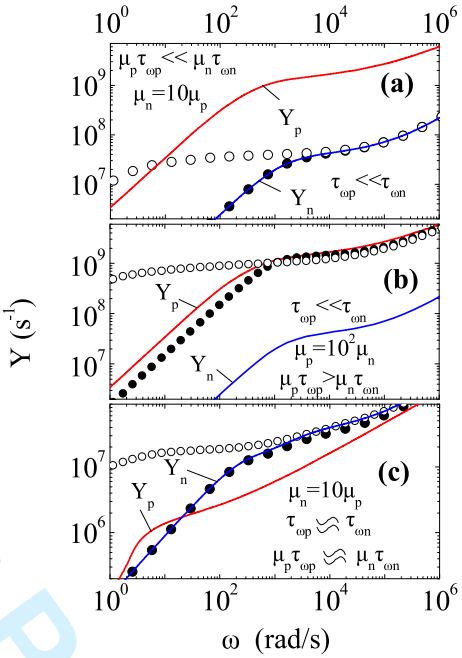

FIG. 5: Calculated Y spectra for a low $n_0 = 1.1 \times 10^7\ cm^{-3}$ (open symbols) and moderate $n = 1 \times 10^{10}\ cm^{-3}$ (solid symbols) for $\mu_n = 10\ cm^2V^{-1}s^{-1}$ using the DOS model of Fig.4 by setting $\mu_p = 0.1\mu_n$ in (a), $\mu_p = 10^2\mu_n$ in (b) and the relatively lower capture coefficients $c_p^v = 10c_n^v = 1 \times 10^{-10}cm^3s^{-1}$ and $\mu_p = 0.1\mu_n$ in (c). The respective Y_n and Y_p spectra calculated for the moderate n are included for comparison.

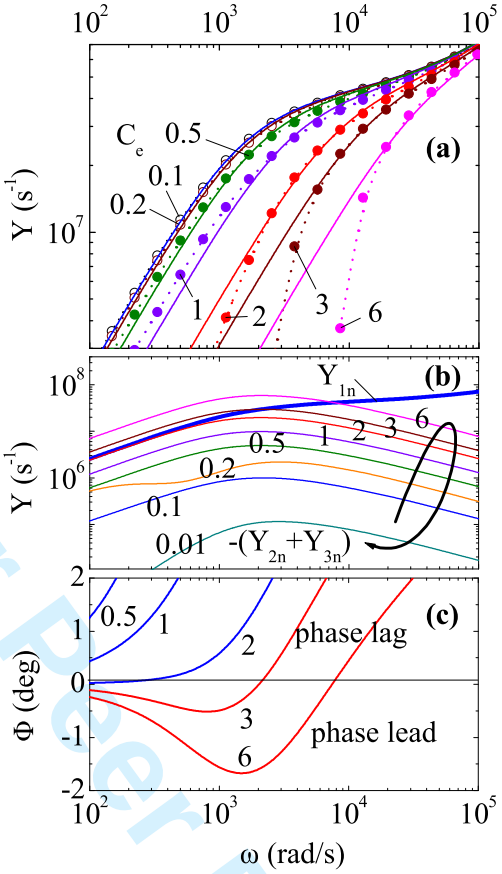

FIG. 6: (a) Y spectra (circles and dotted lines) calculated for $n = 1 \times 10^{10}$ cm^{-3} and the indicated values of C_e in comparison with the respective reconstructed $1/\tau_\omega$ rates (solid lines). (b) Comparison of the Y_{1n} spectrum (thick solid line) with the spectra of the total negative $Y_{2n} + Y_{3n}$ contribution (thin solid lines) for the indicated C_e (numbers). (c) Examples of phase shift lag ($\phi > 0$) and phase shift lead ($\phi < 0$) spectra obtained for the indicated C_e (numbers).

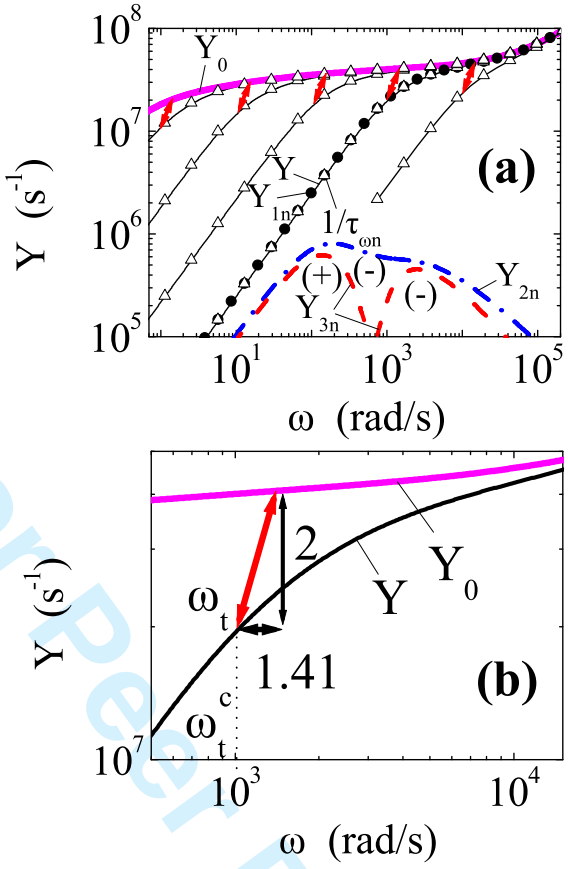

FIG. 7: (a) Calculated spectra of Y (solid lines) and $1/\tau_{\omega n}$ (open triangles) of different densities n (2.9×10^6, $10^7, 10^8, 10^9, 10^{10}$ and 10^{11} cm^{-3} from left to right in the figure). Y_{1n} spectrum (solid circles) in comparison with Y_{2n} (dashed-dotted lines) and Y_{3n} (dashed lines) spectra for the moderate $n = 10^{10}$ cm^{-3}. The signs of the Y_{2n} and Y_{3n} are indicated. The bias light-independent Y_0 spectrum (thick solid line) is obtained with a near dark equilibrium density $n_0 = 2.9 \times 10^6$ cm^{-3}. (b) An example demonstrating the determination of ω_t for the Y signal of $n = 10^{10}$ cm^{-3}. The ω_t is defined as the frequency where the Y signal decreases by the factor of 2 (vertical double arrow) from the respective value in Y_0 spectrum of the same trap depth that is by a factor of 1.41 (horizontal double arrow) above ω_t.

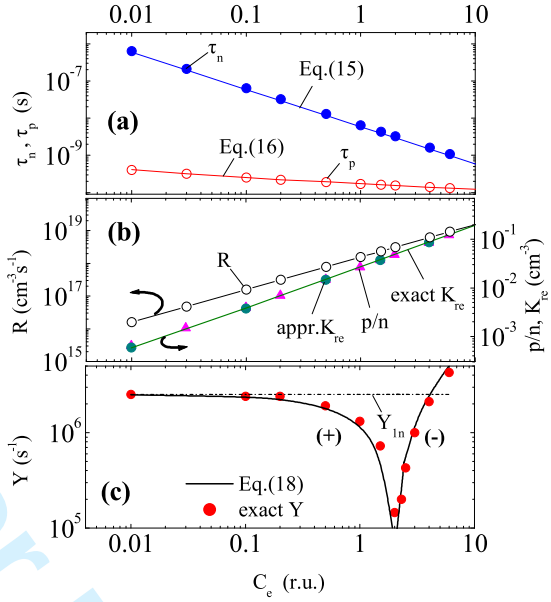

FIG. 8: Exact lifetimes τ_n and τ_p and approximate ones from Eqs.(15) and (16) in (a), recombination rate R, p/n ratio, exact K_{re} from Eq.(A1) and approximate K_{re} from Eq.(A3) in (b) and calculated exact Y signal (solid circles) in comparison with Y signal (solid line) calculated from Eq.(18) in the LF regime ($\omega = 98\ rad/s$) in (c) for a constant $n = 10^{10}\ cm^{-3}$ as a function of C_e.

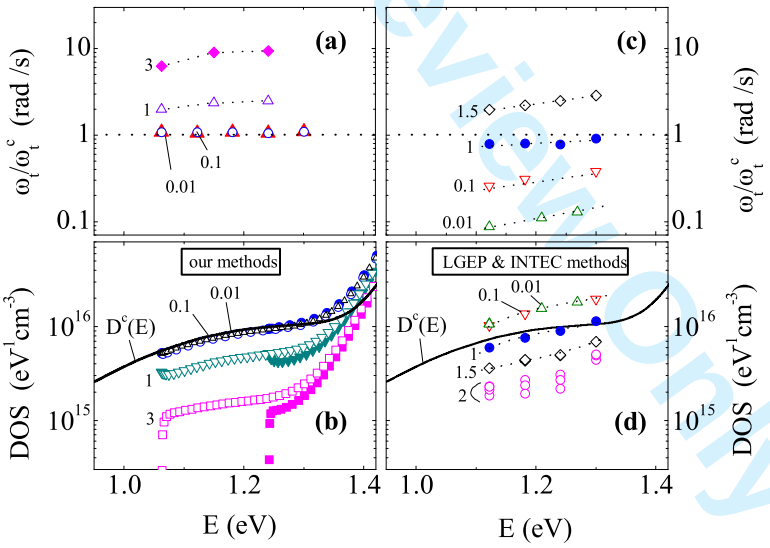

FIG. 9: Normalized reconstructed characteristic frequency ω_t/ω_t^c in (a) and (c) and reconstructed $D(E)$ (symbols) in comparison with the introduced $D^c(E)$ (solid line) in (b) and (d) as a function of the energy for the indicated C_e (numbers), according to our methods ((a) and (b)) and the methods of LGEP and INTEC groups ((c) and (d)).

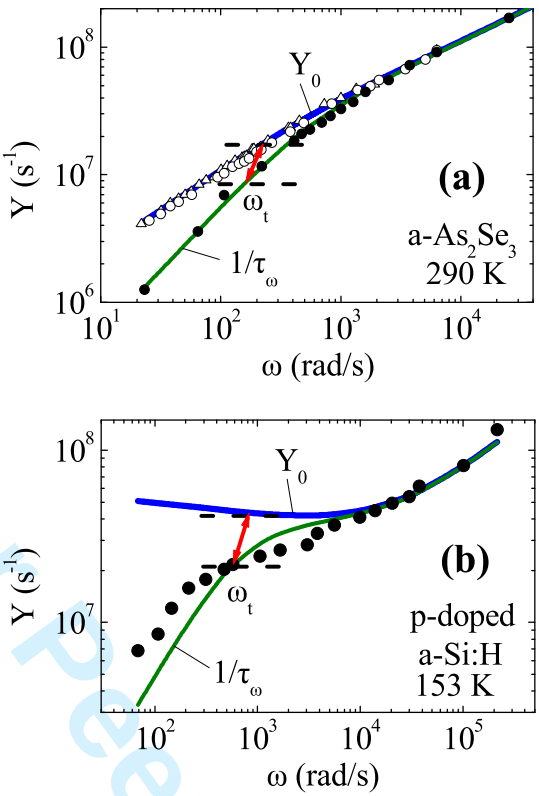

FIG. 10: a) Experimental spectra of Y signal of a-As_2Se_3 sputtered films taken from our previous publication [35] for light intensities of 8.2×10^{11} (open triangles), 3.6×10^{12} (open circles) and 2.8×10^{13} (solid circles) $cm^{-2}s^{-1}$. (b) Experimental spectra of Y and Y_0 spectra extracted from the MPC data of light p-type doped a-Si:H reported by Kleider et al [24]. Each reconstructed $1/\tau_\omega$ rate (solid line) is also included in (a) and (b) for comparison.

FIGURES AND FIGURE CAPTIONS

215x279mm (600 x 600 DPI)